Appl. Phys. A 53, 155–163 (1991)

Applied Physics A Solids and Surfaces

© Springer-Verlag 1991

Microstructure and Thermal Stability of Fe, Ti, and Ag Implanted Yttria-Stabilized Zirconia

B. A. van Hassel and A. J. Burggraaf

Laboratory for Inorganic Chemistry, Materials Science, and Catalysis, Department of Chemical Technology, University of Twente, P.O. Box 217, NL-7500 AE Enschede, The Netherlands

Received 18 December 1990/Accepted 22 March 1991

Abstract. Yttria-stabilized zirconia (YSZ) was implanted with 15 keV Fe or Ti ions up to a dose of 8×10^{16} at cm^{-2}. The resulting "dopant" concentrations exceeded the concentrations corresponding to the equilibrium solid solubility of Fe_2O_3 or TiO_2 in YSZ. During oxidation in air at 400° C, the Fe and Ti concentration in the outermost surface layer increased even further until a surface layer was formed of mainly Fe_2O_3 and TiO_2, as shown by XPS and ISS measurements. From the time dependence of the Fe and Ti depth profiles during anneal treatments, diffusion coefficients were calculated. From those values it was estimated that the maximum temperature at which the Fe- and Ti-implanted layers can be operated without changes in the dopant concentration profiles was 700 and 800° C, respectively. The high-dose implanted layer was completely amorphous even after annealing up to 1100° C, as shown by scanning transmission electron microscopy. Preliminary measurements on 50 keV Ag implanted YSZ indicate that in this case the amorphous layer recrystallizes into fine grained cubic YSZ at a temperature of about 1000° C. The average grain diameter was estimated at 20 nm, whereas the original grain size of YSZ before implantation was 400 nm. This result implies that the grain size in the surface of a ceramic material can be decreased by ion beam amorphisation and subsequent recrystallisation at elevated temperatures.

PACS: 61.70.Tm, 66.30.Jt

Yttria-stabilized zirconia (YSZ) is an important oxygen ion conducting solid electrolyte. It is used in applications like oxygen sensors, oxygen pumps, and fuel cells [1]. Mixed conducting oxides, which show both ionic and electronic conductivity, are considered to be attractive candidates for use as electrode material on top of YSZ [2–4].

The major objective of the present study is to check the possibility to obtain by ion implantation a mixed conducting surface layer in YSZ [5–9] and in this way to investigate the possibility to increase the rate of electrochemical reactions at the gas-solid interface. Fe and Ti have been chosen as dopants since the corresponding oxides are semiconductors at the operating temperature of YSZ [10, 11]. Some studies on the electronic properties of YSZ doped with transition metal oxides have shown that mixed conductivity is obtained. These results, however, depend strongly on temperature, oxygen partial pressure, and dopant concentration [5, 12–15].

Ion implantation has been used as a surface modification technique because the transport of oxygen ions from the ion implanted surface layer into the solid electrolyte can take place very gradually. By, e.g., sputtering of doped YSZ a sharp interface would exist between the sputtered thin film and the solid electrolyte. Such an interface may hinder the transport of oxygen from the mixed conducting surface layer into the solid electrolyte, especially if the mixed conducting layer and the solid electrolyte are not iso-structural.

Transition metal oxides have only limited solid solubility in YSZ. The concentration of the implanted ion that can be obtained by ion implantation is independent of its equilibrium solid solubility level. Concentrations of the transition metal oxide far above its solubility level may be necessary in order to obtain the desired effects.

In this paper we report on the chemical composition of the surface, the thermal stability of the dopant depth profile and the microstructure of the implanted layer. With respect to the microstructure also preliminary results on Ag-implanted YSZ, indicating the influence of the type of implanted ion, are reported. In subsequent papers the electrochemical properties of the ion-implanted layer will be discussed [16].

1. Experimental

Yttria stabilized zirconia powder [Zircar, type: ZYP $(ZrO_2)_{0.87}(YO_{1.5})_{0.13}$] was isostatically pressed (400 MPa) and heated, first for three hours at 1300° C and finally for three hours at 1400° C. Rods were obtained with a density of 5.89 $g\,cm^{-3}$ (=99% of theoretical density). From these rods discs were cut (diameter: 10 mm, thickness: 1 mm). The discs were mechanically polished, first with SiC (29, 9, 7, and 5 μm) and finally diamond paste (7 and 3 μm).

The ion implantations were performed at room temperature in a vacuum of 5×10^{-5} Pa. The YSZ discs were implanted perpendicular to the sample surface at a beam current density of 2 $\mu A\,cm^{-2}$ using the isotope separator of the Laboratory for General Physics (LAN) of the State University of Groningen. For the hot cathode ion source $FeCl_2 \cdot 4\,H_2O$ (Merck, p.a.) was used as feed material for Fe implantations. For the Ti implantation heated TiO_2 (BDH chemicals Ltd) was chlorinated in situ with carbon tetrachloride. In this paper most experiments were performed on YSZ discs, implanted with 15 keV ^{56}Fe or ^{48}Ti up to a dose of 8×10^{16} $at\,cm^{-2}$. Due to the Fe and Ti implantation, the YSZ discs showed respectively a brown metallic and a silver colour. After oxidation at 400° C in air the Fe implanted samples turned orange while the Ti-implanted samples regained their original white colour. The preliminary Ag-implantation experiments were performed at 50 keV up to a dose of 8×10^{16} $at\,cm^{-2}$.

Subsequently the implanted YSZ discs were annealed in a Pt crucible in a preheated furnace in air at temperatures between 800–1400° C. The temperature of the samples was measured close to the Pt crucible with a chromel-alumel thermocouple at temperatures below 1000° C and with a Pt/Pt-10% Rh one above 1000° C.

Rutherford backscattering (RBS) experiments have been performed using the 5 MeV van der Graaff accelerator of the LAN of the State University of Groningen. Depending on the specific depth distribution of the implanted ions, 2 or 3 MeV ^4He ions were used as primary ions. All measurements were carried out with a scattering angle of 165° in the laboratory frame of reference and with an angle of 60° between the surface normal and the incident beam. The surface barrier detector, with an energy resolution of 26 keV (FWHM), was positioned at 75° with respect to the surface normal. With this energy resolution of the detector, a depth resolution of 12 nm (FWHM) was obtained in the described scattering geometry.

As the analyzed depth profiles were rather shallow, the surface energy approximation was used in calculating the stopping- and differential scattering cross sections [17]. From the Fe, Ti, and Zr+Y signal heights, the Fe/(Fe+Zr+Y) and Ti/(Ti+Zr+Y) cation ratios were calculated. The ratio of oxygen atoms to cations was calculated by assuming the number of oxygen atoms to be in stoichiometric ratio with the maximum valence state of the cations (i.e. Fe^{3+}, Ti^{4+}, Y^{3+}, and Zr^{4+}). This assumption holds if the sample is oxidized at 400° C in air. If the oxidation is not performed, than the ion implanted layer is oxygen deficient. The procedure followed here differs from the one used by Scholten et al. [6] and yields slightly different profile shapes.

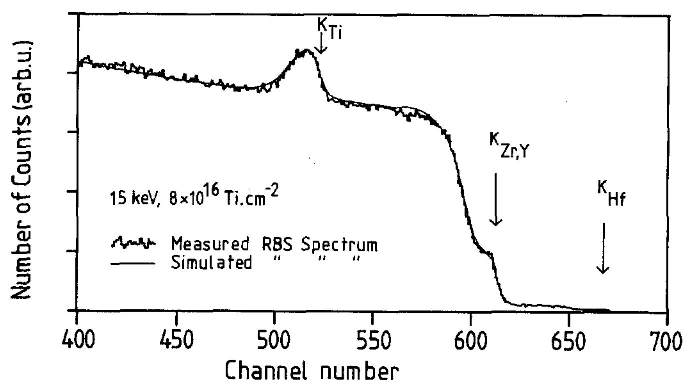

Fig. 1. Experimental RBS spectrum for Ti-implanted YSZ. The spectrum simulated with the "RUMP" [18] programme based on the calculated Ti profile of Fig. 2b

The stopping cross section of the compound YSZ target was calculated from the atomic composition according to Bragg's rule [17], enabling the RBS energy scale to be translated into a depth scale ($at\,cm^{-2}$). The $at\,cm^{-2}$ depth scale was recalculated in nm by assuming that the atomic density had not changed during implantation. No corrections were applied for the limited energy resolution of the surface barrier detector, nor for the range straggling of the scattered ions.

With the computer program RUMP [18], the RBS spectrum was simulated from the calculated Fe or Ti depth profile. As demonstrated by Fig. 1 a good agreement was obtained between the observed and calculated RBS spectrum.

X-ray photoelectron spectroscopy (XPS) measurements were performed with the Kratos X SAM-800 apparatus of the Centre for Materials Science (CMO) of Twente University. The spectra were recorded with Mg-$K_{\alpha 1,2}$ (1253.6 eV) radiation. The photoelectrons were analyzed in a concentric hemisphere analyzer (CHA) which was located perpendicular to the sample's surface. The energy resolution of the CHA was 0.99 eV (FWHM) at the pass energy of 20 eV. Background corrections were applied following the method developed by Shirley [19].

Corrections for surface charging (2–5 V) were applied using the C 1*s* signal (285.1 eV, due to surface impurities) as a reference. This resulted in a binding energy of 530.2 eV for the O 1*s* electron. When the C 1*s* signal disappeared due to sputtering then the O 1*s* signal was taken as a reference.

The sampling depth of the XPS measurements amounts to 2–3 nm. In order to obtain a sputtering depth profile, a 3 keV Ar^+ ion beam was used with a sputter rate of 0.6 $nm\,min^{-1}$ for Ta_2O_5. The corresponding sputter rate for YSZ was calculated by adjusting the value of the sputter rate until a best agreement was obtained between the RBS and XPS depth profile. This resulted in a sputter rate of 0.6 $nm\,min^{-1}$ and 0.43 $nm\,min^{-1}$ for respectively the Fe- and Ti-implanted layers. The depth resolution of the sputter profile is estimated to be within the range of 20–30 nm (FWHM).

Table 1. XPS sensitivity factors, relative to Zr $3d = 1$

Element	Area $2p$	Area $3d$
Zr		1
Y		0.26
Fe	1.64	
Ti	1.37	

For quantitative analysis of the XPS data accurate atomic sensitivity factors had to be obtained [20]. The absolute surface concentration from the RBS spectra could not be used for this purpose as this concentration is unreliable due to the limited energy resolution of the detector. Instead it was assumed that the Fe/(Fe + Zr + Y) and Ti/(Ti + Zr + Y) cation ratio at a depth respectively of 5 and of 8 nm should be the same in both the XPS profiles and the RBS spectra. These depth values were chosen to calibrate the sensitivity factors as the depth profiles were relatively flat at that place. Resulting atomic sensitivity factors, relative to Zr $3d = 1.00$, are shown in Table 1.

Low energy ion scattering (ISS) experiments were performed at the University of Tübingen (FRG) using 1 keV $^4He^+$ as primary ion. Scattered ions were analyzed in a CHA at a scattering angle of 135°. In order to avoid charging the measurements were performed at elevated temperatures using resistive heating of the Pt sample holder.

The microstructure of the ion implanted sample was investigated with a Jeol JEM-200CX scanning transmission electron microscope. After polishing the samples to a thickness of 50 µm, the samples were iron milled (3 keV Ar^+) from the backside until a hole appeared.

2. Results

2.1 Surface Modification

Figure 2 shows typical Fe and Ti depth profiles, as determined by RBS, for samples annealed in air at 400° C for 30 min. A remarkable difference exists between the maximum cation ratio of the Fe and Ti depth profiles (0.50 and 0.70 respectively). The total number of Fe and Ti atoms implanted in the sample, obtained from integration of the depth profiles, is respectively 3×10^{16} and 3.5×10^{16}. The remainder has been sputtered away during ion implantation.

XPS in combination with Ar^+ sputtering was used to determine the Fe or Ti concentration in the first 5 nm of

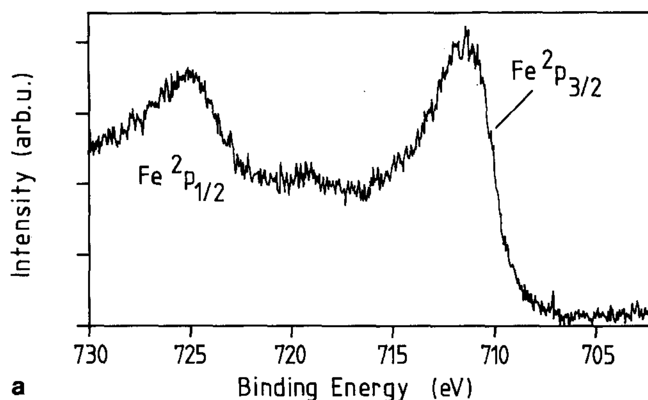

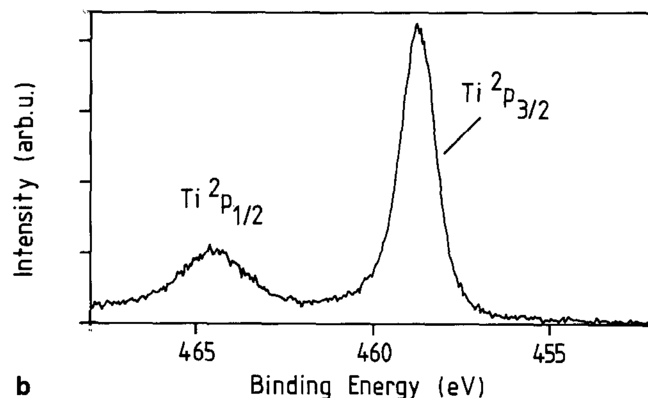

Fig. 3a, b. Core-level XPS spectra for the implanted samples after oxidation at 400° C. **(a)** Fe-implanted YSZ and **(b)** Ti-implanted YSZ, both at standard implantation conditions

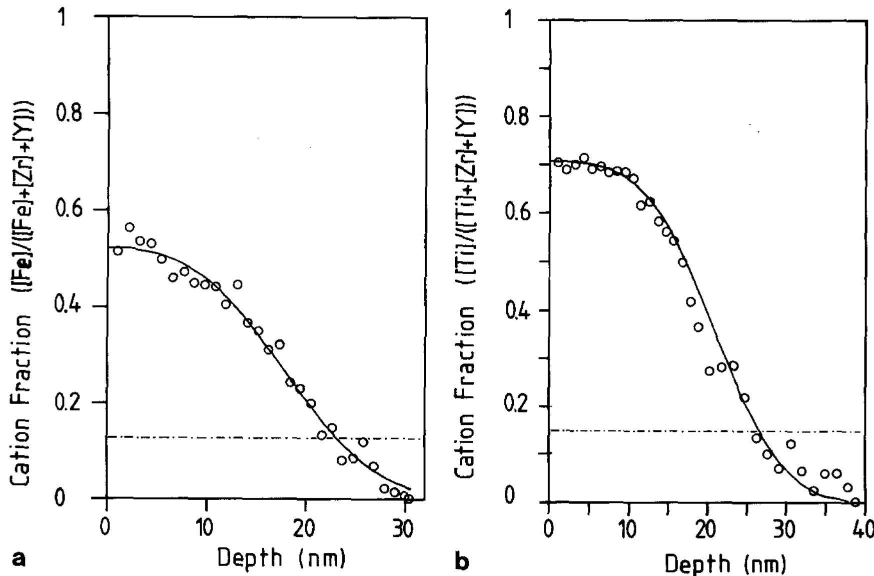

Fig. 2a, b. RBS depth profiles, given as cation fractions, for the implanted ions after oxidation at 400° C, **(a)** for Fe and **(b)** for Ti, both at standard implantation conditions. The solid lines represent the calculated depth profiles of Eq. (1) using the parameters of Table 2. The horizontal broken lines represent the respective solubility limits for Fe and Ti in YSZ (17 cation% Y) at 1500° C in air

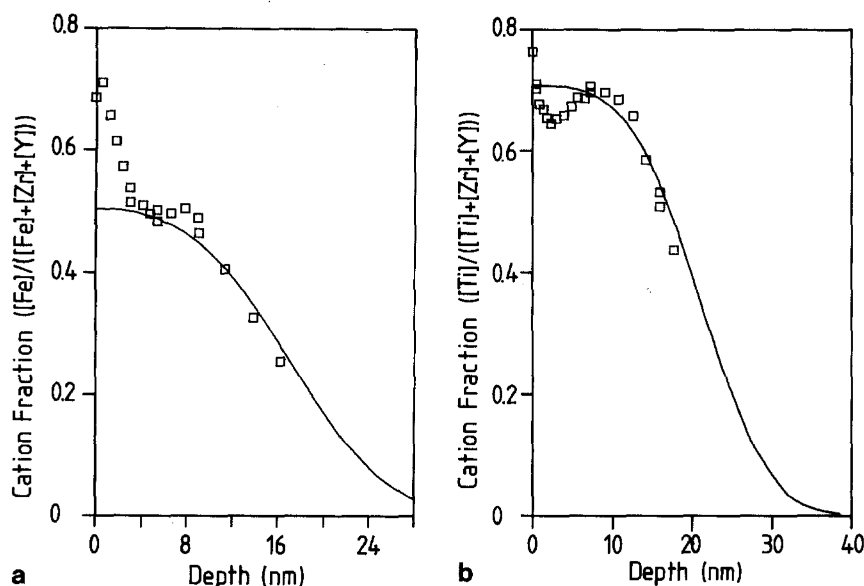

Fig. 4a, b. XPS depth profiles, given as cation fractions, for the implanted ions after oxidation at 400° C, (**a**) for Fe and (**b**) for Ti, both at standard implantation conditions. The solid lines represent the respective RBS depth profiles

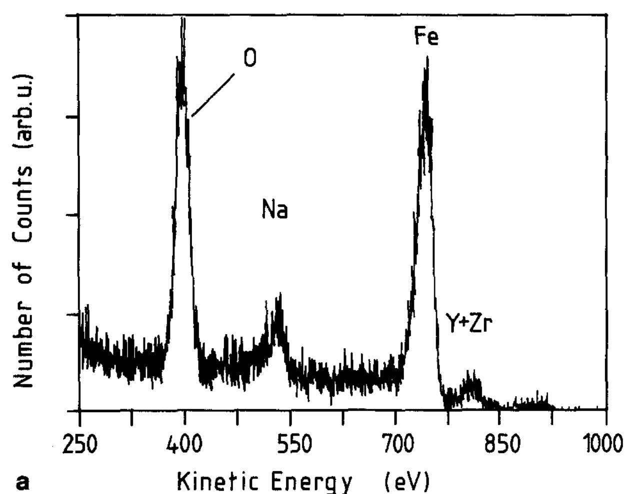

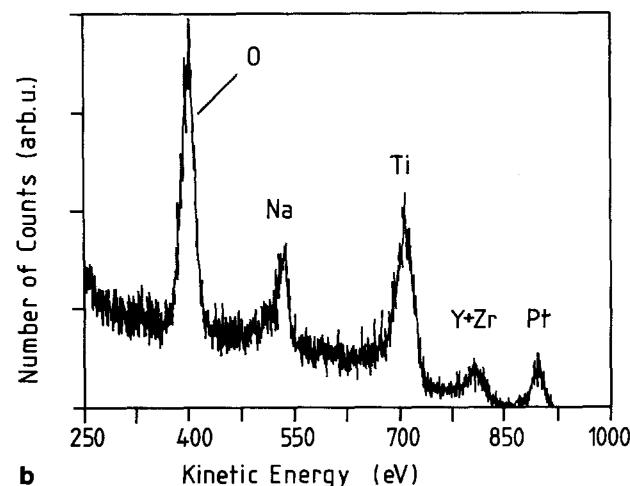

Fig. 5a, b. Low energy ion scattering spectra for the implanted samples after oxidation at 400° C, (**a**) for Fe-implanted YSZ and (**b**) for Ti-implanted YSZ, both at standard implantation conditions

the YSZ sample more carefully (Figs. 3, 4). Fe and Ti depth profiles, as determined by successive Ar^+ ion bombardments followed by XPS analysis are depicted in Fig. 4. The Fe depth profile (Fig. 4a) shows a strong enrichment of the outermost surface layer with Fe extending over 3 nm. A similar result is obtained for Ti implanted YSZ (Fig. 4b). Beyond this Ti-enriched layer at the outermost surface, however, a maximum appears in the Ti depth profile at a depth of 8 nm.

The Fe $2p$ and Ti $2p$ core level XPS spectra of the outermost surface of Fe- or Ti-implanted YSZ are shown in Fig. 3. The binding energy of the

$$\mathrm{Fe}\,2p_{3/2}(711.5 \pm 0.2\ \mathrm{eV}) \quad \text{and} \quad \mathrm{Ti}\,2p_{3/2}(458.7 \pm 0.2\ \mathrm{eV})$$

electrons indicate implanted ions to be present as Fe^{3+} (e.g. Fe_2O_3) and Ti as Ti^{4+} (e.g. TiO_2) [21, 22].

The outermost surface composition was probed by ISS. The ISS spectra, as given in Fig. 5, show the sample surfaces to be slightly contaminated with Na. The Pt signal originates from the sample holder. The most striking result is that in the outermost YSZ surface only O and Fe and almost no Zr or Y are found. Apparently only Fe_2O_3 is present in the outermost surface layer. In the case of the Ti-implanted sample almost no Y or Zr signal is measured and the outermost surface layer mainly consists of TiO_2.

2.2 Thermal Stability

As YSZ is used as an oxygen ion conducting solid electrolyte at high temperatures, the thermal stability of the Fe and Ti depth profiles is of great importance. Therefore the Fe- and Ti-implanted YSZ samples were annealed at temperatures between 800 and 1400° C for a known time (t). Two representative Fe and Ti diffusion profiles, as determined by RBS, are shown in Fig. 6. Within the experimental accuracy, the total number of

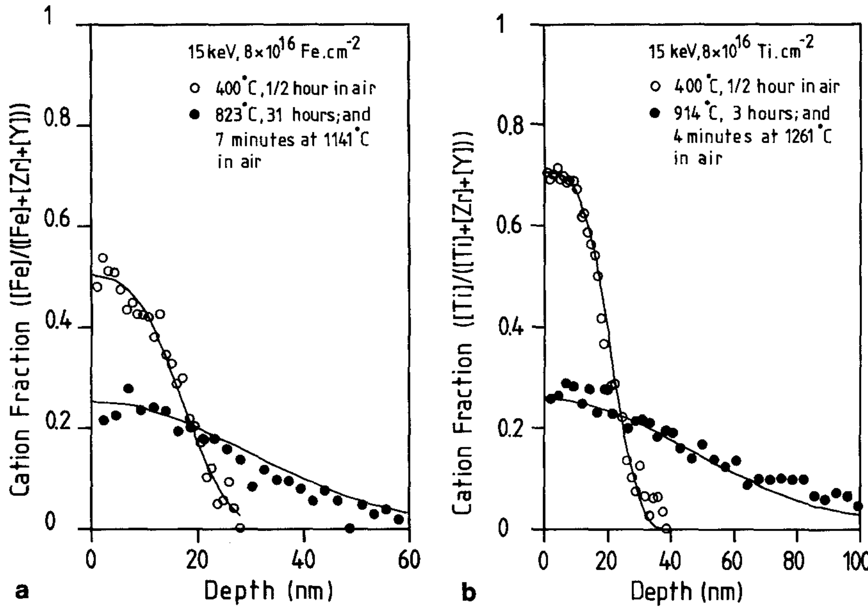

Fig. 6a, b. Change of depth profile of the implanted ions due to diffusion, (**a**) for Fe-implanted YSZ and (**b**) for Ti-implanted YSZ, both implanted under standard conditions

implanted ions remained constant and consequently no significant evaporation of Fe or Ti from the surface had taken place.

Diffusion coefficients, D, were obtained from analysis of the time dependent composition profile during annealing, according to [23]:

$$C(x,t)=\frac{1}{2}C_0\left(\operatorname{erf}\left(\frac{h-x}{2\sqrt{D(t_0+t)}}\right)+\operatorname{erf}\left(\frac{h+x}{2\sqrt{D(t_0+t)}}\right)\right) \quad (1)$$

where:

C_0 = initial concentration of diffusing ion;
h = thickness of the extended source of limited extent;
t_0 = parameter which describes the initial composition profile after ion implantation;
D = diffusion coefficient;
t = diffusion time;
x = space coordinate measured normal to the surface;

This equation describes the concentration-distance curve for the linear diffusion of a source of limited extent into a semi-infinite system. In the derivation of this equation, it has been assumed that no evaporation or trapping occurred at the surface. It has also been assumed that the diffusion coefficient is independent of time, position and concentration and that the initially implanted Fe or Ti concentration is below the solid solubility. The parameters h, C_0, t_0, and D were adjusted to produce best

Table 2. Parameters describing the depth profiles, using Eq. (1), for Fe and for Ti implanted and oxidized YSZ samples

Implanted ion	C_0	h [nm]	Dt_0 [nm²]
Ti	0.69±0.04	19±2	45±6
Fe	0.55±0.03	16±2	37±6

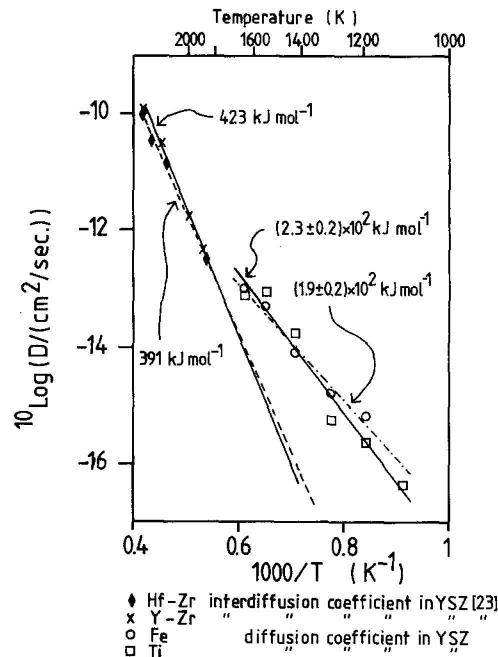

Fig. 7. Comparison between the Y/Zr and Hf/Zr inter-diffusion coefficients in YSZ [24], and the chemical diffusion coefficients of Fe and Ti in YSZ. The diffusion parameters are given in Table 3

agreement between the calculated profile and the measured diffusion profiles in Fig. 6 with the result given by the solid lines. The parameters which describe the initial Fe and Ti depth profiles are summarized in Table 2.

The Arrhenius-plot of the experimentally determined diffusion coefficients of Fe and Ti in YSZ is shown in Fig. 7. Inter-diffusion coefficients of Y/Zr and Hf/Zr in YSZ, such as determined by Oishi et al. [24], are given for comparison. The activation energies and pre-exponential factors for the Fe and Ti diffusion coefficients are given in Table 3.

Table 3. Activation energy (E_{act}) and pre-exponential factor (D_0) for the chemical diffusion coefficient of Fe and Ti in YSZ in comparison with the interdiffusion coefficients of Y/Zr and Hf/Zr [23]. The magnitude of the diffusion coefficient $D(T)$ at a temperature T can be obtained from the Arrhenius equation: $D(T)=D_0 \exp(-E_{act}/RT)$

Diffusing element	D_0 [cm²/s]	E_{act} [kJ/mol]	Temperature range [°C]
Fe	$(1.3 \pm 0.6) \pm 10^{-7}$	$(1.9 \pm 0.2) \times 10^2$	800–1400
Ti	$(3 \pm 2) \times 10^{-6}$	$(2.3 \pm 0.2) \times 10^2$	800–1400
Zr-Hf	0.031	391	1500–2100
Y-Zr	0.27	423	1500–2100

2.3 Microstructure

Although the investigations of the microstructure of the implanted YSZ samples are only preliminary, the results are considered relevant for the discussion of the present data. The Fe- and Ti-implanted layers in YSZ proved to remain amorphous after isochronal annealing for $^1/_2$ hour at temperatures up to 1100° C as indicated by electron diffraction (Fig. 8).

Different results were obtained for (50 keV-) Ag implanted YSZ. After the implantation the originally cubic YSZ matrix also had turned amorphous. Even after isochronal annealing for $^1/_2$ hour at temperatures up to 800° C no crystalline recovery had taken place. After annealing the Ag implanted sample at 1000° C for $^1/_2$ hour, however, the ion implanted layer finally recrystallized into fine grained cubic zirconia. The bright field image and the electron diffraction pattern are shown in Fig. 9. From the bright field image (Fig. 9a) it can be seen that the grain size of the cubic zirconia (originally around 0.4 µm) has been reduced to 20 nm upon recrystallisation at 1000° C. The electron diffraction pattern in Fig. 9b can be indexed with the cubic zirconia phase with a cell parameter of $a=(5.10 \pm 0.05)$ Å which is in fair agreement with the original cell parameter of $a=(5.1358 \pm 0.0002)$ Å as determined by powder X-ray diffraction (XRD). The metallic Cu reflections in Fig. 9b originate from the copper deposited from the Cu sample holder onto the sample surface during "ion milling". Ag could not be detected by energy dispersive analysis of X-rays (EDAX) indicating the evaporation of silver from the surface and/or rapid diffusion into the YSZ lattice.

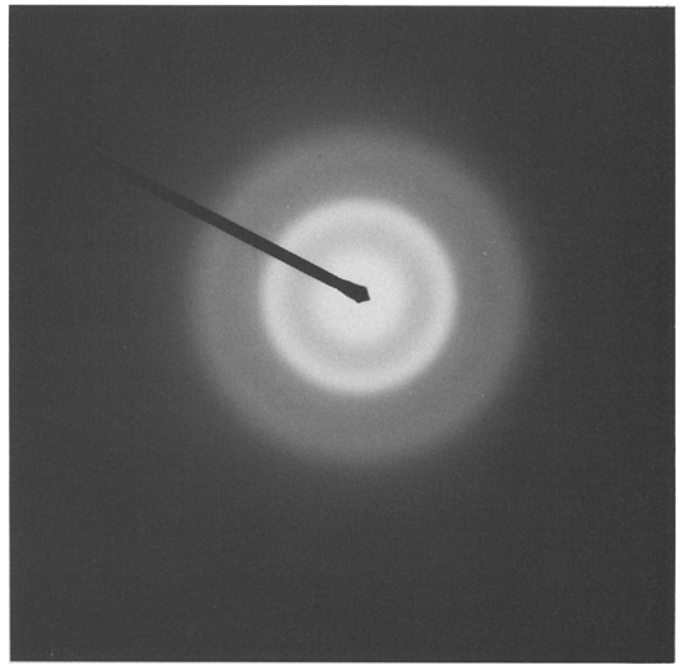

Fig. 8. Electron diffraction pattern of Fe-implanted YSZ (standard conditions and oxidized at 400° C)

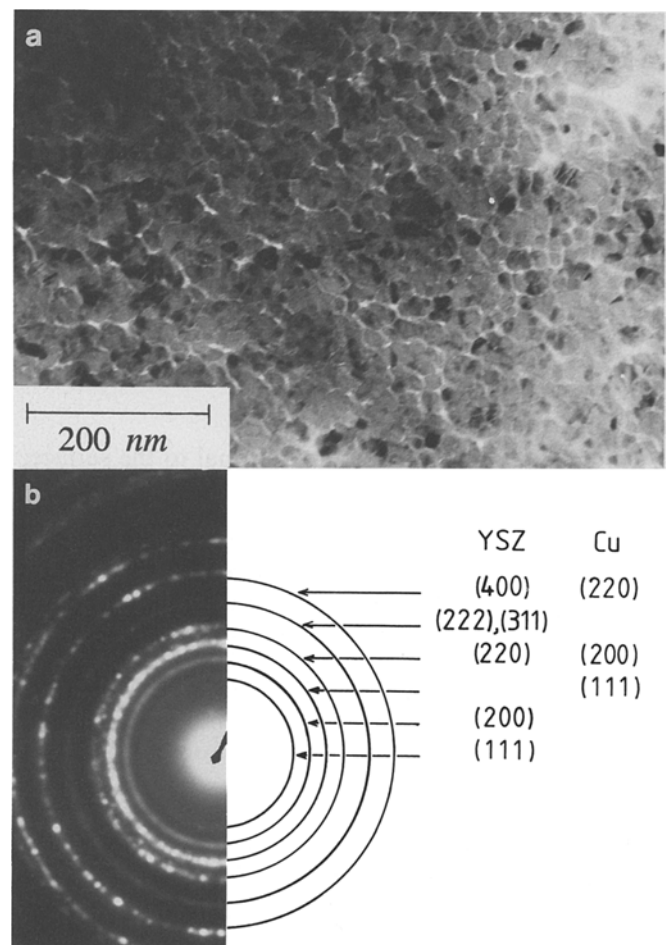

Fig. 9a, b. STEM micrographs of Ag-implanted YSZ (50 keV Ag at a dose of 8×10^{16} at cm^{-2} and annealed at 1000° C in air for $^1/_2$ hour). (**a**) Bright field image and (**b**) electron diffraction pattern of the implanted and recrystallized layer

3. Discussion

The difference in the maximum Fe and Ti concentration in Fig. 2 after implantation under identical conditions is somewhat unexpected. It should be recalled, however, that the maximum concentration in the depth profile originates from a steady state, in which as many ions are implanted as sputtered away. The maximum concentration of the implanted ion is inversely proportional to its sputter yield (number of atoms i sputtered away per incident ion) in the compound target [25]. Apparently the sputter yield of Fe ions during ion implantation is higher than for Ti ions.

The higher sputter yield of Fe ions in comparison to Ti ions during ion implantation is difficult to explain. During depth profiling with 3 keV Ar^+ no preferential sputtering of Fe with respect to Zr was observed [8]. This was assumed to be also valid for Ti atoms. Under these conditions, however, oxygen was found to sputter preferentially with respect to the cations. As a result the transition metal cations were reduced while the Zr oxidation state was less effected. The oxidation state of Fe and Ti in the oxidized implanted layer changed respectively from Fe^{3+} to Fe^{2+} and metallic Fe^0, and from Ti^{4+} to Ti^{3+} and Ti^{2+} upon Ar^+ ion bombardment.

This preferential sputtering of oxygen also occurs during Fe [26, 27] and Ti implantation in YSZ. The concentration of the remaining oxygen is related to the oxidation state of the implanted ions in such a way that the charge of the cations will be compensated with O^{2-} ions. A large fraction of the implanted Fe ions was present in metallic precipitates after high dose implantation [26] whereas from XPS measurements it could be concluded that the implanted Ti ions were mainly present as Ti^{4+}, Ti^{3+}, and Ti^{2+}. As Fe showed a large tendency to form metallic precipitates, the oxygen content of the Fe implanted layer will be lower than for the Ti-implanted layer in the steady state. This will result in a larger sputter yield of Fe ions in comparison to Ti ions.

Moreover, the sputtering rate is related to the mass of the implanted ion. The higher the mass the higher the sputtering rate will be. The mass difference between Fe and Ti, however, is considered too small in order to explain the observed difference in the maximum cation ratio.

The Fe and Ti depth profiles as determined by XPS (Fig. 3) show an enrichment of the implanted ions in the outermost surface layer. As substantiated by ISS, the outermost surface layer consisted mainly of Fe_2O_3 and TiO_2 after oxidation at 400° C in air. In the "as-implanted" state, the intensity of the Y and Zr signal in the ISS spectrum was about four times as high as in the "oxidized" state, indicating a further enrichment with Fe and Ti upon annealing in an oxidizing atmosphere.

This surface enrichment should not be confused with interfacial segregation [28, 29]. Segregation is an equilibrium process and the oxidation temperature of 400° C is considered to be too low in order to obtain equilibrium. Similar driving forces, however, may be responsible for the surface enrichment of Fe and Ti during the oxidation at 400° C in air. A strong effect of the anneal atmosphere on the redistribution of implanted ions during annealing has been observed before by McHargue et al. [37] in the case of Fe implanted Al_2O_3. A profound redistribution of Fe towards the surface occurred during annealing in an oxidizing atmosphere, but not in a reducing atmosphere.

The calculated diffusion coefficients (Fig. 7) are considerably higher than the extrapolated values of the Y/Zr and Hf/Zr inter-diffusion coefficients in YSZ, such as determined by Oishi et al. [24]. This different behaviour may be due to the difference in ionic radii between the diffusing cations (Ti^{4+}: 0.68 Å, Fe^{3+}: 0.64 Å, Zr^{4+}: 0.79 Å, Y^{3+}: 0.89 Å [30]). Oishi et al. [24] found that the smaller the cation, the lower the activation energy for cation self diffusion in YSZ. This can explain the difference in activation energy for the chemical diffusion coefficient of Ti^{4+} and Fe^{3+} in comparison to Y^{3+} and Zr^{4+} in YSZ. The difference may be explained in part by the fact that the implanted layer is disordered. Vacancies and interstitials have been created on both the anion and cation sublattice. The surface changed from a crystalline into an amorphous state during ion bombardment. The diffusion coefficients in disordered solids are generally higher than in crystalline structures [31].

In the analysis of the time dependent concentration-distance curves a number of assumptions have been made, which have to be taken into account before definite conclusions can be drawn. First it was assumed that the diffusion coefficient is independent of time, position, and concentration. The time and position independence is usually an adequate approximation for the post implantation case [32]. The concentration independence is questionable as we are not dealing with dilute solutions of Fe_2O_3 or TiO_2 in YSZ. Secondly it was assumed that the Fe and Ti concentrations were below their levels of solid solubility, which is not the case. It has been found by XRD analysis and application of Vegards law that the equilibrium solubility level of Fe and Ti in cubic YSZ amounts to respectively 7 mol% Fe_2O_3 and 15 mol% TiO_2 at 1500° C in air. These solubility levels have been indicated in Fig. 2 by the horizontal lines. As the limited solubility of the implanted ions has not been taken into account, the calculated diffusion coefficients will be too small. The Fe or Ti concentration gradient, which is the driving force for diffusion, has been overestimated by taking the maximum concentration in the depth profile instead of the much lower equilibrium solid solubility. It may, however, be questioned in how far the equilibrium solubility level of Fe_2O_3 or TiO_2 in YSZ can be used for high dose Fe- or Ti-implanted YSZ, since the lattice became highly disordered and amorphous. Only after recrystallization of the amorphous layer or when the diffusion tail penetrates in the crystalline YSZ region, then the solubility level will be relevant.

The use of high Fe and Ti concentrations in determining diffusion coefficients has been forced by the RBS technique. It is very difficult to detect small concentrations of a light element in a heavy matrix. As the RBS technique is essentially nondestructive, consecutive diffusion annealing experiments could be performed on a single sample.

In analogy with ion-implanted metals [32], annealing of the high dose implanted samples should result in precipitation when the solubility limit is exceeded. Prolonged annealing then would lead to the dissolution of the precipitates accompanied by transport of the implanted ions into the single phase bulk. This transport should start from its equilibrium solid solubility level. A sharp discontinuity in the slope of the concentration-distance curve is then expected at the boundary between the one and two phase region. The large scatter in the calculated concentration-distance curve or the limited depth resolution of the RBS spectrum may be responsible for the fact that such a discontinuity, if present, could not be detected in the Fe and Ti diffusion profiles of Fig. 6.

For (electrochemical) characterization and possible applications it is important to establish the maximum temperature at which the profile does not significantly change over a prolonged period of time. Based on the Fe and Ti depth profiles of Fig. 2, and the condition that a maximum decrease of 10% in the surface concentration of the implanted ion can be allowed, the diffusion coefficient must be less than $10^{-17}\,cm^2\,s^{-1}$. Extrapolation of the Arrhenius plot of Fig. 7 then leads to a maximum operation temperature of 700° C for Fe, and 800° C for Ti-implanted YSZ. The decrease in surface concentration is not linear with time, after an initial rapid decrease the decrease will diminish due to a flattening of the initially steep concentration gradient.

The amorphisation of ZrO_2 by ion bombardment has been questioned for a long time [27, 33]. Electron diffraction patterns of Fe and Ti implanted YSZ showed that YSZ turned amorphous after high dose implantation. The same result was obtained for Ag-implanted YSZ.

As previously reported, the recrystallisation of an amorphous layer depends strongly on the implanted ion [9]. An important step in the recrystallisation process is the nucleation of a crystalline phase. Legg et al. [36] concluded that the nucleation and crystal growth temperature ranges for alumina precipitates in Al-implanted YSZ were well separated. Slow heating through the nucleation temperature range (1150–1250° C) resulted in a nucleation controlled microstructure consisting of interconnected alumina precipitates on top of YSZ. The recrystallization of an amorphous YSZ layer was studied by Cohen et al. [34] in the case of Yb-implanted YSZ. The amorphous YSZ layer recrystallized epitaxially upon annealing.

In this paper it has been shown that amorphous YSZ, which resulted from the implantation of Ag, recrystallized at 1000° C in small and randomly oriented crystallites with a cubic crystal structure. The crystallization of YSZ ($(ZrO_2)_{0.87}(YO_{1.5})_{0.13}$) mainly into a cubic phase is in agreement with the phase diagram of YSZ [35]. After annealing at temperatures up to 1100° C for $^1/_2$ hour Fe- and Ti-implanted YSZ were still amorphous. Probably, the crystallization is delayed by the absence of nucleation. No precipitation of second phases has yet been observed, despite the fact that, even at 800° C, the inter-diffusion coefficient and annealing time should be considered large enough ($\sqrt{(Dt)} = 3$ nm) in comparison to the lateral resolution of the transmission electron microscope. The evaporation of implanted Ag from the sample surface may explain the absence of any metallic Ag precipitates in ZrO_2. Such precipitates have been observed by Abouchacra et al. [38] in Ag-implanted MgO. In their case (180 keV Ag^+, 5×10^{16}–10^{17} at cm^{-2} in MgO) the ions were implanted deep under the surface (mean projected range = 141 nm).

4. Conclusions

The implantation of 15 keV Fe or Ti ions up to a dose of 8×10^{16} at cm^{-2} results in a diffusion like depth profile with a thickness of 20 nm. The maximum Fe and Ti concentrations correspond to a cation fraction of 0.50 and 0.70, respectively, as shown by RBS. The maximum concentration of the dopant depth profile is located at the surface due to a steady state situation in which as many ions are implanted as sputtered away. The concentration difference between the Fe and Ti depth profiles is caused by a lower sputtering rate for the Ti-implanted layer in comparison to the Fe-implanted layer. During oxidation in air at 400° C, the Fe or Ti concentration in the outermost surface layer (0–2 nm) increases even further until mainly Fe_2O_3 or TiO_2 is present, as shown by XPS in combination with ISS.

The diffusion of Fe or Ti ions in the YSZ matrix is thermally activated with activation energies of $(1.9 \pm 0.2) \times 10^2$ and $(2.3 \pm 0.2) \times 10^2$ kJ/mol, respectively. Based on the experimentally determined Fe and Ti diffusion coefficients it is concluded that the maximum operating temperatures at which the implanted dopant profiles are still stable in time are about 700 and 800° C, respectively. At higher temperatures the diffusion of Fe or Ti takes place into deeper layers of the polycrystalline YSZ matrix.

The implantation of 15 keV Fe and Ti or 50 keV Ag up to a dose of 8×10^{16} at cm^{-2}, results in a complete amorphisation of the YSZ matrix, as shown by scanning transmission electron microscopy. After isochronal annealing for $^1/_2$ hour at temperatures between 400 and 1100° C the Fe- and Ti-implanted samples remained amorphous. The Ag-implanted sample recrystallised at 1000° C into cubic zirconia with a mean grain diameter of about 20 nm, whereas the original bulk grain diameter amounted to 400 nm. From this result it can be concluded that the grain size of polycrystalline ceramic materials can be decreased by ion beam amorphisation and subsequent recrystallisation at elevated temperatures.

Acknowledgement. The authors appreciate the cooperation with the "Laboratorium voor Algemene Natuurkunde (LAN)" of the State university of Groningen. They are grateful to J. J. Smit for the ion implanter facilities. They thank Dr. D. O. Boerma of the state university of Groningen for his supervision during the RBS measurements, and A. Vredenberg (Amolf/Amsterdam) for the introduction to the computer program RUMP. They are indebted to Ing. A. H. J. van den Berg of the Centre for Materials Science of Twente University for measuring the XPS depth profiles. They appreciate also the cooperation with the "Institut für Physikalische und Theoretische Chemie" of the university of Tübingen (Federal Republic of Germany) and thank U. Vohrer for performing the ISS measurements. Dr. Ir. J. Beyer is thanked for the close examination of the microstructural changes in YSZ with the STEM. The investigations were supported by the Netherlands Foundation for Chemical Research (SON) with financial aid from the Netherlands Organization for Scientific Research (NWO).

References

1. E.C. Subbarao, H.S. Maiti: Solid State Ionics **11**, 317 (1984)
2. M.P. van Dijk: PhD Thesis, University of Twente, Enschede, The Netherlands (1985)
3. M.P. van Dijk, K.J. de Vries, A.J. Burggraaf: Solid State Ionics **21**, 73 (1986)
4. Y. Takasu, T. Sugini, Y. Matsuda: J. Appl. Electrochem. **14**, 79 (1984)

5. D. Scholten: Surface modification of yttria stabilized zirconia by ion implantation, PhD Thesis, University of Twente, Enschede, The Netherlands (1987)
6. D. Scholten, A.J. Burggraaf: Radiat. Eff. **97**, 191 (1986)
7. D. Scholten, A.J. Burggraaf: Surf. Interface Anal. **9**, 467 (1986)
8. D. Scholten, A.J. Burggraaf: Solid State Ionics **16**, 147 (1985)
9. B.A. van Hassel, A.J. Burggraaf: Appl. Phys. A **49**, 33 (1989)
10. B.M. Warnes, F.F. Aplan, G. Simkovich: Solid State Ionics **12**, 271 (1984)
11. B. Poumellec, J.F. Marucco, F. Langel: Phys. Status Solidi A **89**, 375 (1985)
12. V.K. Gil'derman, A.D. Neuimin, S.F. Pal'guev, Yu.S. Toropov: Élektrokhimiya **12**, 1585 (1976)
13. Yu.N. Karavaev, A.D. Neuimin, S.F. Pal'guev: Élektrokhimiya **23**, 121 (1987)
14. W.L. Worrell: Solid State Ionics **28–30**, 1215 (1988)
15. S.S. Liou, W.L. Worrell: Appl. Phys. A **49**, 25 (1989)
16. B.A. van Hassel: Transport and oxygen transfer properties of ion implanted yttria stabilized zirconia, PhD Thesis, University of Twente, Enschede, The Netherlands (1990)
17. Wei-Kan Chu, J.W. Mayer, M.-A. Nicolet: *Backscattering Spectrometry* (Academic, New York 1978)
18. L.R. Doolittle: Nucl. Instrum. Meth. B **9**, 344 (1985)
19. D.A. Shirley: Phys. Rev. B **5**, 4709 (1972)
20. M. Grasserbauer, H.J. Dudek, M.F. Ebel (eds.): *Angewandte Oberflächen Analyse mit SIMS, AES, XPS* (Springer, Berlin, Heidelberg 1985)
21. A. Fujimori, M. Saeki, N. Kimizuka, M. Taniguchi, S. Suga: Phys. Rev. B **34**, 7318 (1986)
22. S. Hofmann, J.M. Sanz: J. Trace Microprobe Techniques **1**, 213 (1982–83)
23. J. Crank: *The Mathematics of Diffusion*, 2nd edn. (Clarendon, Oxford 1975)
24. Y. Oishi, K. Ando, Y. Sakka: In *Advances in Ceramics*, Vol. 7, ed. by M.F. Yan, A.H. Heuer (American Ceramic Society, Columbus, Ohio 1983) pp. 208–219
25. H. Ryssel, I. Ruge: *Ion Implantation* (Wiley, Chichester 1986)
26. A.J. Burggraaf, D. Scholten, B.A. van Hassel: Nucl. Instrum. Meth. B **32**, 36 (1988)
27. J.A. Sawicki, G. Marest, B. Cox: In *Structure-Property Relationships in Surface-Modified Ceramics, NATO ASI Series E: Applied Sciences-Vol. 170*, ed. by C.J. McHargue, R. Kossowsky, W.O. Hofer (Kluwer, Dordrecht 1989) pp. 209–218
28. P. Wynblatt, R.C. McCune: In *Surface and Near-Surface Chemistry of Oxide Materials, Materials Science Monographs*, Vol. 47, ed. by J. Nowotny, L.-C. Dufour (Elsevier, Amsterdam 1988) pp. 247–279
29. A.J. Burggraaf, A.J.A. Winnubst: In *Surface and Near-Surface Chemistry of Oxide Materials, Materials Science Monographs*, Vol. 47, ed. by J. Nowotny, L.-C. Dufour (Elsevier, Amsterdam 1988) pp. 449–477
30. CRC Handbook of Chemistry and Physics, 67th edn., ed. by R.C. Weast (CRC, Florida 1989)
31. P. Mazzoldi, A. Miotello: In *Structure-Property Relationships in Surface-Modified Ceramics, NATO ASI Series E: Applied Sciences*, Vol. 170, ed. by C.J. McHargue, R. Kossowsky, W.O. Hofer (Kluwer, Dordrecht 1989) pp. 27–45
32. S.M. Myers: In *Ion Implantation, Treatise on Materials Science and Technology*, Vol. 18, ed. by J.K. Hirvonen (Academic, New York 1980) pp. 51–83
33. R. Kelly: In *Ion Bombardment Modification of Surfaces, Fundamentals, and Applications, Beam Modification of Materials 1*, ed. by O. Aucielli, R. Kelly (Elsevier, Amsterdam 1984)
34. C. Cohen, J. Siejka, M. Berti, A.V. Drigo, M. Croset, M.M. Tosci: Radiat. Eff. **64**, 221 (1982)
35. H.G. Scott: J. Mater. Sci. **10**, 1527 (1975)
36. K.O. Legg, J.K. Cochran Jr., H.F. Solnick-Legg, X.L. Mann: Nucl. Instrum. Meth. B **7/8**, 535 (1985)
37. C.J. McHargue, G.C. Farlow, P.S. Sklad, C.W. White, A. Perez, N. Kornilios, G. Marest: Nucl. Instrum. Meth. B **19/20**, 813 (1987)
38. G. Abouchacra, J. Serughetti: Nucl. Instrum. Meth. B **14**, 282 (1987)